sciendo

DFT studies of camptothecins cytotoxicity IV — active and inactive forms of irinotecan

Marek Štekláč, Martin Breza

Department of Physical Chemistry, Faculty of Chemical and Food Technology STU, Radlinského 9, SK-81237, Bratislava, Slovakia
martin.breza@stuba.sk

Dedicated to Assoc. Prof. Jozef Kožíšek on the occasion of his 70th birthday.

Abstract: Structures of irinotecan (CPT-11) in neutral lactone, neutral carboxyl, and anionic carboxylate forms in singlet ground states and of their complexes with Cu(II) in doublet ground states are optimized using B3LYP/6-311G* treatment. Metal ion affinities (MIA), Cu charges and Laplacians of Cu-ligand bond critical points of possible CPT active sites are evaluated. The formation of Cu(II) complexes with the anionic carboxylate ligand leads to the release of CO_2 that can cause a decrease in the concentration of the active lactone form due to equilibria between all forms of the drug. MIA values and electron density transfer to Cu increase in the sequence lactone < neutral carboxyl < anionic carboxylate. Both neutral forms of irinotecan exhibit lower MIA values than those of camptothecin, unlike the anionic carboxylate form.

Keywords: copper(II), cytotoxicity, DFT calculations, electron structure, molecular modelling

Introduction

The semisynthetic anticancer drug irinotecan (CPT-11), (4*S*)-4,11-diethyl-3,4,12,14-tetrahydro-4-hydroxy-3,14-dioxo-1*H*-pyrano[3',4':6,7]-indolizino[1,2-b]quinolin-9-yl-[1,4'-bipiperidine]-1'-carboxylate was approved for cancer treatment in 1994 (Bailly, 2019). It is obtained by chemical modification of camptothecin with the aim to increase its low water solubility (Sawada et al., 1991). After enzymatic cleavage of the bispiperidine side chain, its minor metabolite SN-38, (4*S*)-4,11-diethyl-4,9-dihydroxy-1,4-dihydro-3*H*,14*H*-pyrano[3',4':6,7] indolizino[1,2-*b*]quinolone-3,14-dione is obtained, which is an even more potent anticancer drug (Tanizawa et al., 1994). In aqueous solutions, the lactone ring of irinotecan is hydrated to the inactive carboxylate form, which is favored under neutral and alkaline conditions, whereas the active lactone form **I** prevails in acidic solutions (Fassberg and Stella, 1992; DiNunzio et al., 2018). Structure of the irinotecan lactone form has been determined by single crystal X-ray diffraction (Sawada et al., 1991), NMR measurements in DMSO solution (D'Amelio et al., 2012), and quantum-chemical model studies (Babu et al., 2012; Ivanova and Spiteller, 2012; Hussain et al., 2016).

Relative cytotoxicity of various forms of camptothecin and lactone forms of irinotecan and SN-38 have been investigated in a series of studies (Steklac and Breza, 2018, 2021, 2022, 2022a) by means of quantum chemistry. This treatment was originally developed for antioxidants (Alagona and Ghio, 2009, 2009a; Mammino, 2013; Kabanda et al., 2014; Tsiepe et al., 2015; Serobatse et al., 2016, 2016a; Puskarova and Breza, 2016, 2017; Jelemenska and Breza, 2021; Breza and Jelemenska, 2022) and is based on the complexation ability of their various active sites to Cu(II) with subsequent electron density transfer (ligand oxidation and metal reduction). Metal ion affinity (*MIA*) data for the ligand active sites in hypothetical complexes can be obtained by DFT treatment. However, inclusion of the solvent effect decreases the *MIA* values and thus, vacuum model studies are more suitable for cytotoxicity studies (Alagona and Ghio, 2009, 2009a; Mammino, 2013).

This method has been successfully applied to rutile nanoparticles (Breza and Simon, 2019, 2020; Breza, 2021), substituted phenols (Steklac and Breza, 2021a, 2021b) and benzoquinones (Steklac and Breza, 2021c) revealing linear relations between the degree of electron density transfer to Cu, Cu-phenol interaction energy and experimental toxicity data, which were evaluated as $\log(1/IC_{50})$ where IC_{50} is the concentration of substituted phenol/benzoquinone that causes 50 % inhibition of cell growth.

The generally accepted paradigm that the purpose of quantum-chemical modelling is to explain the properties of real systems is usually interpreted so that only real systems should be modelled. This is a very restricted interpretation. Our method of modelling hypothetical complexes to compare the complexation ability and the extent of electron density transfer for individual active sites of the compound under study is an example of extended interpretation of this paradigm. In our case, the

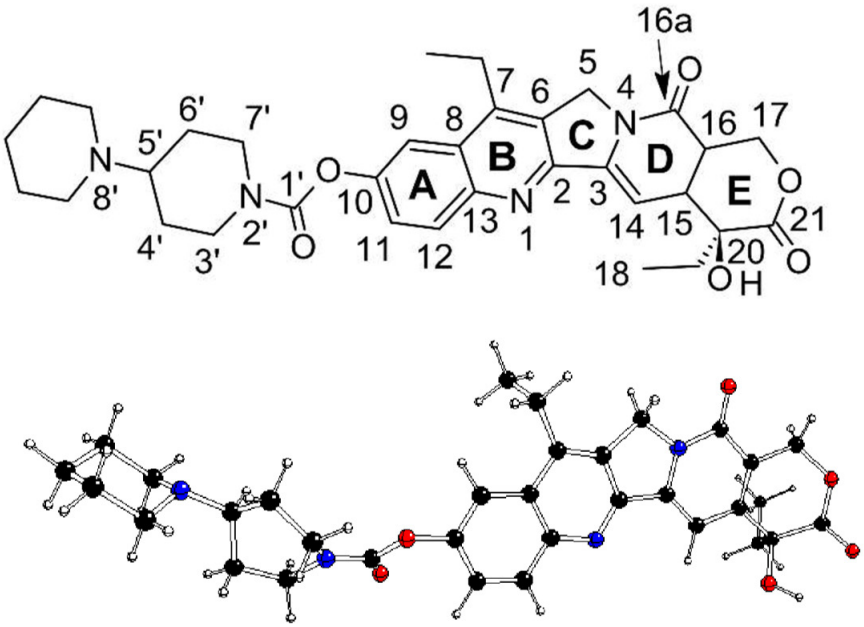

Fig. 1. Atom and ring notation of the irinotecan (CPT-11) lactone (top) and the DFT structure (bottom) of its neutral form **I** (carbon — black, hydrogen — white, nitrogen — blue, oxygen — red) studies (Steklac and Breza, 2022a).

Cu^{2+} ion serves only as a probe to measure properties of the complexes and to rationalize the electronic structure factors of cytotoxicity. This is of practical importance as experiments cannot distinguish between pharmacokinetics and electronic structure factors of the drug action.

In our studies (Steklac and Breza, 2021, 2022), we have explained why the carboxylate and protonated lactone forms of camptothecin are not suitable as anticancer drugs. In our previous comparative study (Steklac and Breza, 2022a), cytotoxicity of lactone forms was found to decrease in the sequence irinotecan > SN-38 > camptothecin. The discrepancy with the least relative *in vitro* irinotecan cytotoxicity is probably due to their different pharmacokinetics. The aim of our recent study is to compare the cytotoxicity of the neutral lactone, neutral carboxyl, and anionic carboxylate forms of irinotecan, which coexist in aqueous solutions. In agreement with our previous cytotoxicity studies, all calculations were performed *in vacuo* because of more palpable trends compared to solutions (see above).

Method

Geometries of three forms of irinotecan (neutral lactone and carboxyl, anionic carboxylate) in singlet ground states, as well as of their Cu(II) complexes in doublet ground state, were optimized using the B3LYP hybrid functional (Becke, 1993). Standard 6-311G* basis sets from the Gaussian library (Frisch et al., 2013) were used for all atoms. Optimized geometries were checked for the absence of imaginary vibrations by vibrational analysis. The charges and spin populations of copper atoms were evaluated using the Mulliken population analysis (MPA) (Mulliken, 1955, 1955a). Gaussian09 software was used for all quantum-chemical calculations (Frisch et al., 2013).

Alternatively, the charge and spin population of copper was evaluated in terms of Quantum Theory of Atoms-in-Molecules (QTAIM) (Bader, 1990). Irinotecan → Cu electron density transfer was estimated as the Laplacian of the electron density ($\nabla^2\rho$) at bond critical points (BCP) using the AIMAll software (Keith, 2017). The MOLDRAW software (Ugliengo, 2006) was used for geometry manipulation and visualization purposes. QTAIM molecular graphs were drawn using the AIM2000 software (Biegler-Konig et al., 2001).

Metal-ion affinity (*MIA*) was evaluated as the interaction energy

$$E_{int} = E_{complex} - E_{Cu(II)} - E_{L} \quad (1)$$

where $E_{complex}$ is the DFT energy of the $^2[L...Cu]^{2+q}$ complex, $E_{Cu(II)}$ is the DFT energy of the copper(II) ion and E_L is the DFT energy of the L ligand, i.e., the neutral lactone (q = 0), neutral carboxyl (q = 0) or anionic carboxylate (q = −1) form of irinotecan.

Results and discussion

In the first step, structures of neutral lactone (**I**), neutral carboxyl (II), and three possible anionic car-

boxylate (**III**) forms of irinotecan were optimized. After hydration of the lactone ring (Fig. 1), the C_{21}—O_{17} bond is split, the O_{21} site is formally doubled, and the O_{17} site is protonated to the neutral carboxyl form **II** (Fig. 2). Subsequently, this form can be deprotonated at the O_{17}, O_{20}, or O_{21} sites. Our results show that the most probable deprotonation site is at O_{21} (see Table 1) and that only this isomer should be present in real systems. Therefore, only this structure will be denoted as form **III** (Fig. 3) and considered in our further studies.

Tab. 1. Absolute (G_{298}) and relative (ΔG_{298}) Gibbs energies at 298 K of the deprotonated irinotecan carboxylate forms (**III**) at various sites and their relative abundance (P_i) based on Boltzmann statistical distribution.

Site	G_{298} [Hartree]	ΔG_{298} [kJ/mol]	P_i
O_{17}	–2026.46179	218.42	5.41×10^{-39}
O_{20}	–2026.50356	108.75	8.85×10^{-20}
O_{21}	–2026.54498	0.00	1.00

In the next step, a Cu^{2+} ion was placed in the vicinity of heteroatoms (ca 1.7 Å distance) of the above mentioned molecules, i.e., N_1 (**a**), N_4 (**b**), O_{16a} (**c**), O_{20} (**d**), O_{21} (**e**), O_{17} (**f**), O_{10} (**g**), $O_{1'}$(**h**), $N_{2'}$(**i**) or $N_{8'}$(**j**) sites in model complexes with ligands **I**, **II** and **III** in agreement with our previous studies (Steklac and Breza, 2021, 2022, 2022a). Thus obtained geometry optimization of the ^{2}[L...Cu]^q complexes leads to stable structures with QTAIM molecular graphs presented in (Steklac and Breza, 2022a) for L being the neutral lactone **I** ligand (q = +2), in Figs. 4—5 for L being the neutral carboxyl ligand **II** (q = +2), and in Figs. 6—7 for L being the anionic carboxylate ligand **III** (q = +1). Notation of these complexes (see Table 2) is related to the Cu-bond sites mentioned above.

No model complexes with Cu bound to the N_4 site have been found. Similarly as in the case of camptothecin (Steklac and Breza, 2021), the Cu—O_{17} bonding is absent in case of neutral lactone ligand **I** and the formation of Cu(II) complexes with carboxylate form **III** leads to the release of CO_2 (except for models **IIIe** and **IIIef** with Cu—O_{21} bonding, see Table 2 and Figs. 6—7). Interactions with neighboring electron-accepting molecules can decrease electron density at the relevant active sites of carboxylate forms of camptothecins and cause their decarboxylation (and decay) and therefore contribute to the decrease in the concentrations of the active lactone form (Steklac and Breza, 2021).

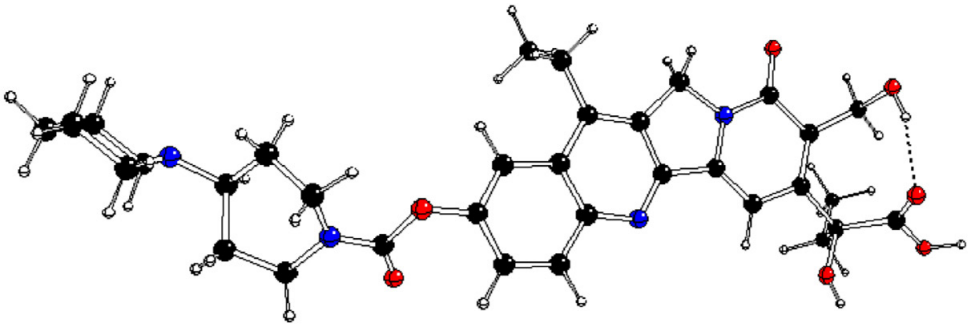

Fig. 2. DFT structure of neutral irinotecan carboxyl **II** (carbon — black, hydrogen — white, nitrogen — blue, oxygen — red).

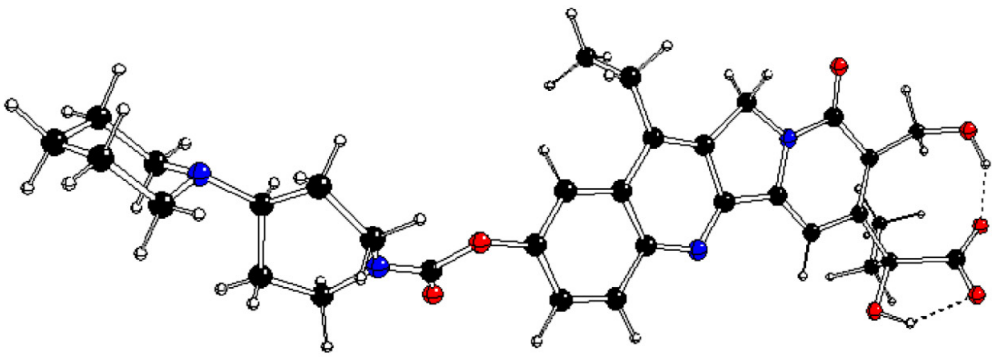

Fig. 3. DFT structure of anionic irinotecan carboxylate **II** (carbon — black, hydrogen — white, nitrogen — blue, oxygen — red).

If the Cu atom is bound to a single atom only, the extent of the corresponding electron density transfer from the active site to Cu can be accurately evaluated. Unfortunately, such cases are rare, and the Cu atom is often bound to two atoms. The H atom basis sets were not augmented with any polarization and diffusion functions in order to weaken the undesirable Cu—H bonds (collateral with desired Cu—O or Cu—N bonds), their lengths are greater than 2.2 Å (except for the **Ig** and **IIg** systems) and so the H contribution to the complete electron density transfer to Cu are usually very small (compare (Steklac and Breza, 2021, 2022, 2022a)). Unfortunately, undesirable Cu—C bonding (collateral with desired Cu—O bonding) with shorter bond lengths (comparable to the Cu—O ones) and a relevant C → Cu electron density transfer (compare (Steklac and Breza, 2021, 2022, 2022a)) is problematic and pure contributions of the active O sites to complete electron density transfer to Cu cannot be distinguished. Therefore, the **Id**, **IIId**, **Ih**, **IIh**, **IIIh** and **IIef**2 systems are hardly usable for our purpose. Even though in the systems with Cu bound to two or three O sites (**IIcf**, **IIIcf**, **IIef1,** and **IIIef**), their pure contributions cannot be separated, they can at least be used for mutual comparisons of carboxyl and carboxylate ligands.

In our studies on the cytotoxicity of substituted phenols (Steklac and Breza, 2021a, 2021b, 2021c),

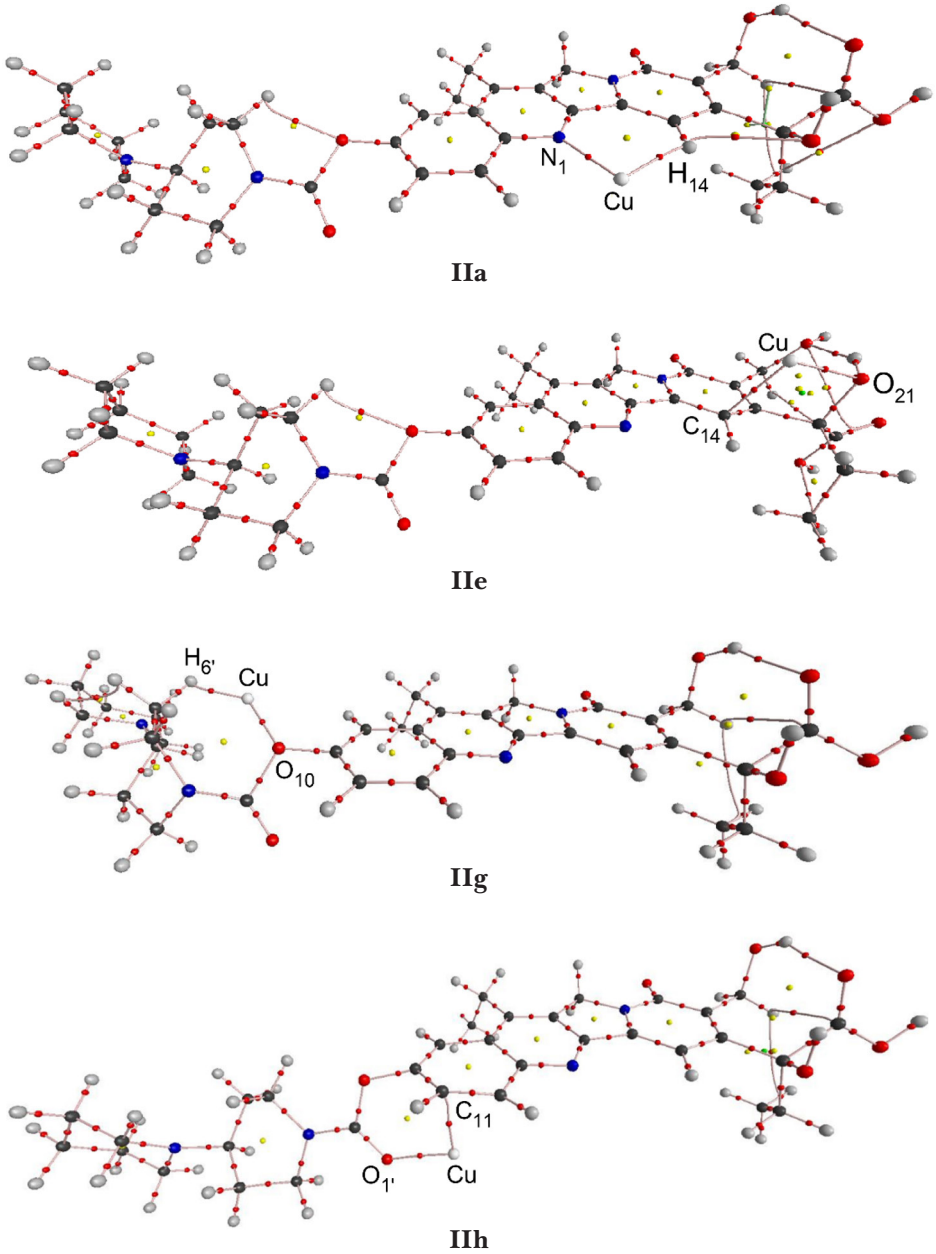

Fig. 4. Bond paths and critical points of electron density in **IIa**, **IIe**, **IIg**, and **IIh** model systems (carbon — black, hydrogen — white, nitrogen — blue, oxygen — red, bond critical point — small red, ring critical points — yellow, cage critical point — green).

higher toxicity was shown to be connected with more negative interaction energies E_{int}. According to our results (Table 3), E_{int} values for the neutral irinotecan carboxyl ligand **II** are more negative than for the neutral lactone ligand **I**, but significantly less negative than for the anionic carboxylate ligand **III**. An analogous relation has been observed for camptothecin (Steklac and Breza, 2021). Both neutral forms of camptothecin exhibit less negative E_{int} values than irinotecan, unlike the negative carboxylate form. As expected, bonding to two O sites is connected with more negative E_{int} values than in

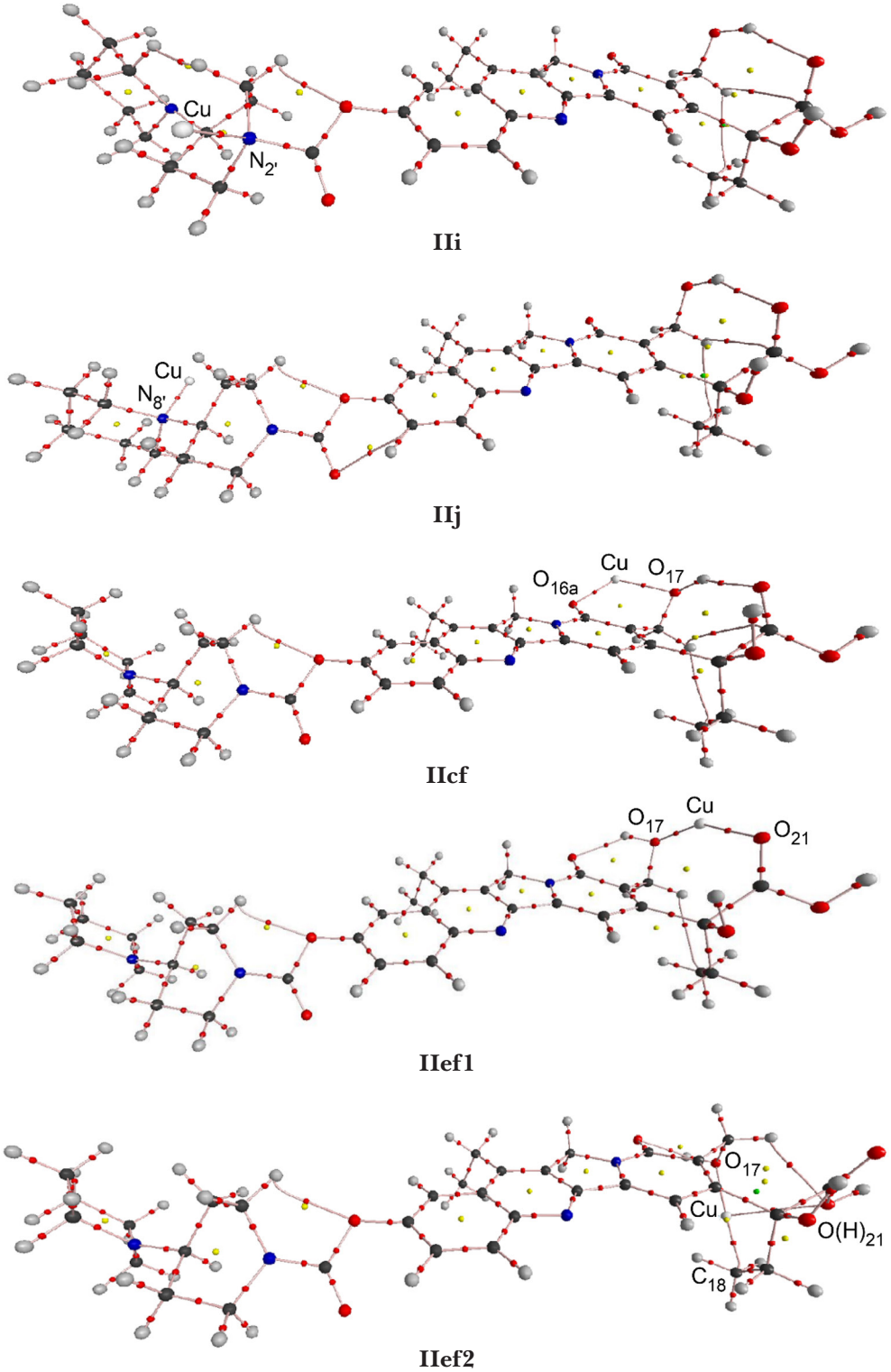

Fig. 5. Bond paths and critical points of electron density in **IIi**, **IIj**, **IIcf**, **IIef1**, and **IIef2** model systems (carbon — black, hydrogen — white, nitrogen — blue, oxygen — red, bond critical point — small red, ring critical points — yellow, cage critical point — green).

the case of bonding to a single O site only. The least negative E_{int} values were found for Cu—O_{10} and Cu—$N_{2'}$ bonds, which are missing in analogous camptothecin systems (Steklac and Breza, 2021).

Positive QTAIM charges of copper atoms in the Cu(II) complexes with substituted phenols decrease with their cytotoxicity due to increasing ligand → Cu electron density transfer (Steklac and Breza, 2021a, 2021b, 2021c). Analogously to our previous study on camptothecin (Steklac and Breza, 2021), average Cu charges in the complexes with the anionic irinotecan carboxylate ligand **III** are lower than in case of neutral irinotecan lactone **I** and carboxyl **II** ligands (Table 4). Nevertheless, the lowest Cu charges correspond to **IIIi** and **IIIj** systems (missing in camptothecin complexes), whereas the most positive Cu charges are found in **IIId** and **IIIef** complexes. Unlike camptothecin complexes, non-vanishing Cu spin populations can be found only in anionic irinotecan carboxylate complexes **IIId**, **IIIi**, **IIIj**, and **IIIef**.

BCP Laplacians of Cu-ligand bonds in Cu complexes of substituted phenols (Steklac and Breza, 2021a, 2021b, 2021c) increase with their toxicity. Their values for Cu—H bond paths are very low (Table 5)

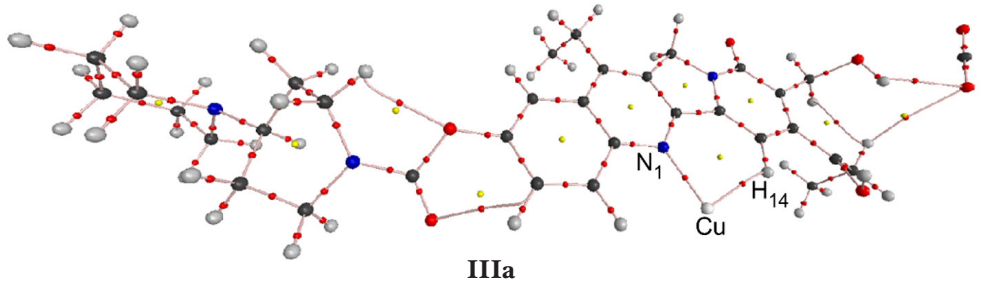

IIIa

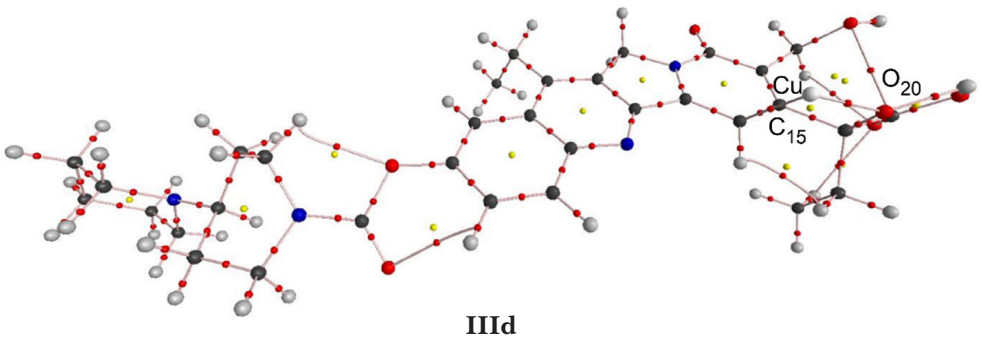

IIId

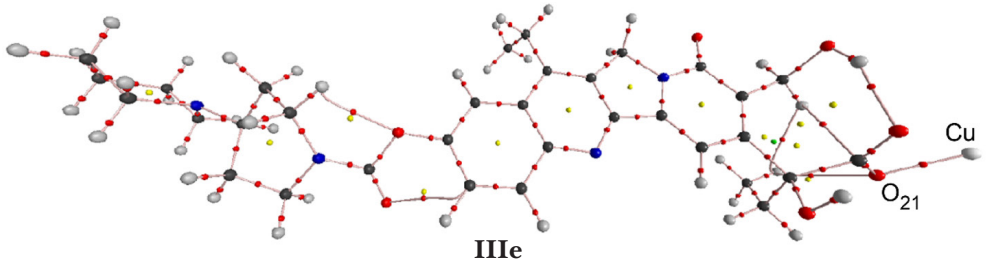

IIIe

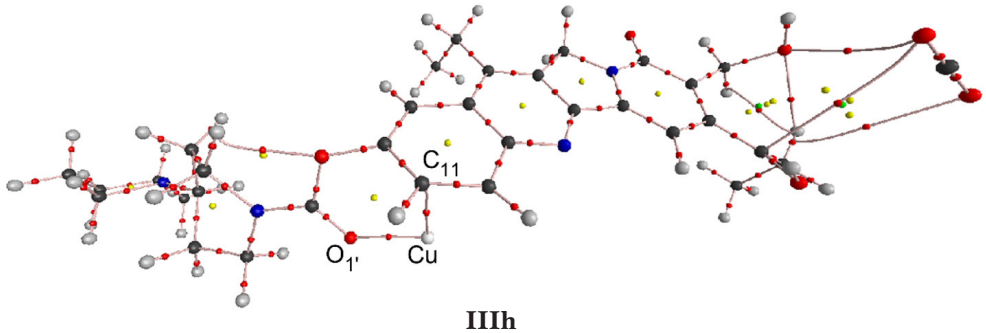

IIIh

Fig. 6. Bond paths and critical points of electron density in **IIIa**, **IIId**, **IIIe**, and **IIIh** model systems (carbon — black, hydrogen — white, nitrogen — blue, oxygen — red, bond critical point — small red, ring critical points — yellow, cage critical point — green).

except for **Ig** and **IIg** complexes with too short bond lengths. BCP Laplacians of Cu—C bonds are relatively high in comparison with the Cu—O ones, restricting the use of the **Id**, **IIId**, **IIe**, **Ih**, **II**h, **IIIh** and **IIef**2 complexes for our purpose. Our results indicate the highest electron density transfer from the O_{21} and O_{16a} sites, while the lowest one from $N_{2'}$, $N_{8'}$, and O_{10} sites.

Similarly to camptothecin (Steklac and Breza, 2021), most trends of MPA charges of Cu atoms in Cu(II) complexes of various forms of irinotecan (Table 6) are similar to those of QTAIM. Cu charges of anionic carboxylate **III** complexes are lower than those of the complexes with neutral ligands **I** and **II**. Except for the **IIIef** system, the highest Cu charges are found in the complexes with Cu—C bonds. The lowest Cu charges are observed for **IIIi** and **IIIj** complexes with Cu—N bonds to piperidine rings. Non-vanishing Cu spin populations are again observed in **IIId**, **IIIi**, **IIIj** and **IIIef** complexes of the

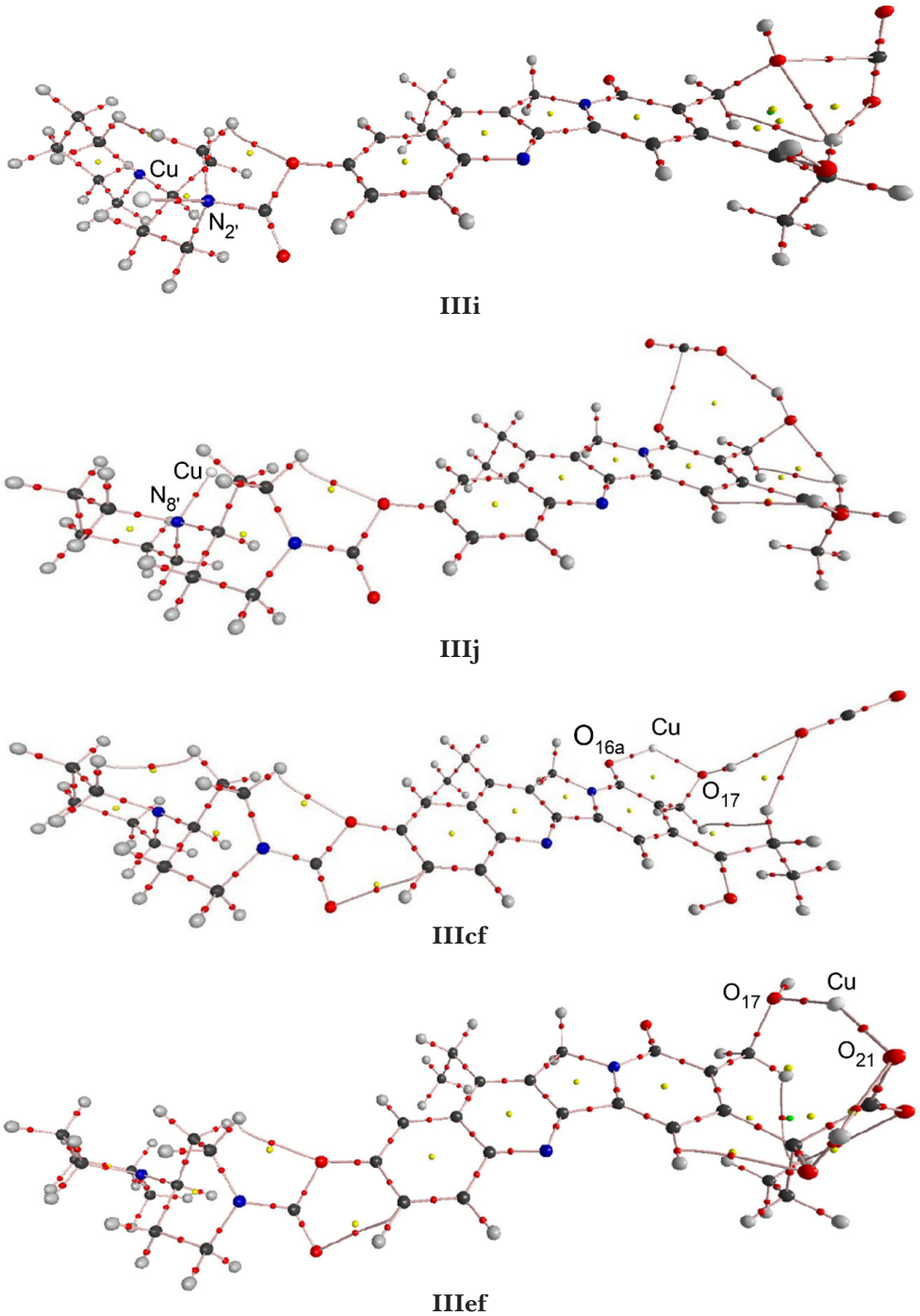

Fig. 7. Bond paths and critical points of electron density in **IIIi**, **IIIj**, **IIIcf**, and **IIIef** model systems (carbon — black, hydrogen — white, nitrogen — blue, oxygen — red, bond critical point — small red, ring critical points — yellow, cage critical point — green).

Tab. 2. Description of Cu model complexes with lactone (**I**), carboxyl (**II**), and carboxylate (**III**) ligands (see Fig. 1 for atom notation).

	I (Steklac and Breza, 2022)			**II**			**III**		
Site	Model	Bond path	Distance [Å]	Model	Bond path	Distance [Å]	Model	Bond path	Distance [Å]
N_1	**Ia**	Cu—N_1 Cu—H_{14}	1.879 2.223	**IIa**	Cu—N_1 Cu—H_{14}	1.877 2.208	**IIIa**[a)]	Cu—N_1 Cu—H_{14}	1.867 2.288
O_{16a}	**Ic**	Cu—O_{16a} Cu—H_5	1.830 2.542	–	–	–	–	–	–
O_{20}	**Id**	Cu—O_{20} Cu—C_{14}	2.061 1.988	–	–	–	**IIId**[a)]	Cu—O_{20} Cu—C_{15}	1.839 2.020
O_{21}	**Ie**	Cu—O_{21}	1.865	**IIe**	Cu—O_{21} Cu—C_{14}	2.081 2.031	**IIIe**	Cu—O_{21}	1.848
O_{10}	**Ig**	Cu—O_{10} Cu—$H_{6'}$	1.954 1.674	**IIg**	Cu—O_{10} Cu—$H_{6'}$	1.954 2.066	–	–	–
$O_{1'}$	**Ih**	Cu—$O_{1'}$ Cu—C_{11}	1.977 1.982	**IIh**	Cu—$O_{1'}$ Cu—C_{11}	1.970 1.981	**IIIh**[a)]	Cu—$O_{1'}$ Cu—C_{11}	1.956 1.986
$N_{2'}$	**Ii**	Cu—$N_{2'}$	1.925	**IIi**	Cu—$N_{2'}$	1.923	**IIIi**[a)]	Cu—$N_{2'}$	1.965
$N_{8'}$	**Ij**	Cu—$N_{8'}$	1.927	**IIj**	Cu—$N_{8'}$	1.927	**IIIj**[a)]	Cu—$N_{8'}$	1.952
O_{16a}, O_{17}	–	–	–	**IIcf**	Cu—O_{16a} Cu—O_{17}	1.909 1.962	**IIIcf**[a)]	Cu—O_{16a} Cu—O_{17}	1.885 1.945
O_{17}, O_{21}	–	–	–	**IIef1**	Cu—O_{17} Cu—O_{21}	1.906 1.870	**IIIef**	Cu—O_{17} Cu—O_{21}	1.895 1.832
	–	–	–	**IIef2**	Cu—O_{17} Cu—$O(H)_{21}$ Cu—C_{18}	1.926 2.597 2.128	–	–	–

[a)]CO_2 release

Tab. 3. Interaction energies in model complexes of Cu with lactone (**I**), carboxyl (**II**) and carboxylate (**III**) ligands (see Fig. 1 for atom notation).

	I (Steklac and Breza, 2022)		**II**		**III**	
Site	Model	E_{int} [kJ/mol]	Model	E_{int} [kJ/mol]	Model	E_{int} [kJ/mol]
N_1	**Ia**	–1368	**IIa**	–1378	**IIIa**[a)]	–1975
O_{16a}	**Ic**	–1338	–	–	–	–
O_{20}	**Id**	–1369	–	–	**IIId**[a)]	–1890
O_{21}	**Ie**	–1353	**IIe**	–1404	**IIIe**	–1905
O_{10}	**Ig**	–1219	**IIg**	–1255	–	–
$O_{1'}$	**Ih**	–1376	**IIh**	–1397	**IIIh**[a)]	–2040
$N_{2'}$	**Ii**	–1225	**IIi**	–1255	**IIIi**[a)]	–1901
$N_{8'}$	**Ij**	–1364	**IIj**	–1395	**IIIj**[a)]	–1997
O_{16a}, O_{17}	–	–	**IIcf**	–1464	**IIIcf**[a)]	–2060
O_{17}, O_{21}	–	–	**IIef1**	–1479	**IIIef**	–1976
	–	–	**IIef2**	–1461	–	–
Average	–	–1326		–1388		–1968

[a)]CO_2 release

Tab. 4. QTAIM charges and spin populations of Cu atoms in model complexes of Cu with lactone (**I**), carboxyl (**II**) and carboxylate (**III**) ligands (see Fig. 1 for atom notation).

	I (Steklac and Breza, 2022)			**II**			**III**		
Site	Model	Charge	Spin	Model	Charge	Spin	Model	Charge	Spin
N_1	**Ia**	0.744	0.000	**IIa**	0.739	0.000	**IIIa**[a)]	0.719	0.000
O_{16a}	**Ic**	0.780	0.000	–	–	–	–	–	–
O_{20}	**Id**	0.742	0.001	–	–	–	**IIId**[a)]	0.902	0.343
O_{21}	**Ie**	0.815	0.000	**IIe**	0.740	0.001	**IIIe**	0.727	0.000
O_{10}	**Ig**	0.764	0.000	**IIg**	0.821	0.000	–	–	–
$O_{1'}$	**Ih**	0.800	0.002	**IIh**	0.800	0.002	**IIIh**[a)]	0.782	0.001
$N_{2'}$	**Ii**	0.750	–0.001	**IIi**	0.747	–0.001	**IIIi**[a)]	0.496	0.288
$N_{8'}$	**Ij**	0.678	0.000	**IIj**	0.677	0.000	**IIIj**[a)]	0.491	0.222
O_{16a}, O_{17}	–	–	–	**IIcf**	0.797	0.028	**IIIcf** [a)]	0.756	0.010
O_{17}, O_{21}	–	–	–	**IIef1**	0.770	0.001	**IIIef**	0.857	0.188
	–	–	–	**IIef2**	0.727	0.000	–	–	–
Average	–	0.759	0.000	–	0.758	0.003	–	0.716	0.132

[a)]CO_2 release

Tab. 5. Laplacians of BCP electron density of Cu-ligand bonds in model complexes of Cu with lactone (**I**), carboxyl (**II**) or carboxylate (**III**) ligands (see Fig. 1 for atom notation).

	I (Steklac and Breza, 2022)			**II**			**III**		
Site	Model	Bond path	$\nabla^2\rho$ [e/bohr^5]	Model	Bond path	$\nabla^2\rho$ [e/bohr^5]	Model	Bond path	$\nabla^2\rho$ [e/bohr^5]
N_1	**Ia**	Cu—N_1 Cu—H_{14}	0.513 0.068	**IIa**	Cu—N_1 Cu—H_{14}	0.515 0.070	**IIIa**[a)]	Cu—N_1 Cu—H_{14}	0.521 0.060
O_{16a}	**Ic**	Cu—O_{16a} Cu—H_5	0.664 0.040	–	–	–	–	–	–
O_{20}	**Id**	Cu—O_{20} Cu—C_{14}	0.346 0.192	–	–	–	**IIId**[a)]	Cu—O_{20} Cu—C_{15}	0.599 0.163
O_{21}	**Ie**	Cu—O_{21}	0.627	**IIe**	Cu—O_{21} Cu—C_{14}	0.563 0.327	**IIIe**	Cu—O_{21}	0.636
O_{10}	**Ig**	Cu—O_{10} Cu—$H_{6'}$	0.492 0.256	**IIg**	Cu—O_{10} Cu—$H_{6'}$	0.492 0.262	–	–	–
$O_{1'}$	**Ih**	Cu—$O_{1'}$ Cu—C_{11}	0.449 0.215	**IIh**	Cu—$O_{1'}$ Cu—C_{11}	0.460 0.215	**IIIh**[a)]	Cu—$O_{1'}$ Cu—C_{11}	0.480 0.221
$N_{2'}$	**Ii**	Cu—$N_{2'}$	0.423	**IIi**	Cu—$N_{2'}$	0.439	**IIIi**[a)]	Cu—$N_{2'}$	0.366
$N_{8'}$	**Ij**	Cu—$N_{8'}$	0.430	**IIj**	Cu—$N_{8'}$	0.434	**IIIj**[a)]	Cu—$N_{8'}$	0.415
O_{16a}, O_{17}	–	–	–	**IIcf**	Cu—O_{16a} Cu—O_{17}	0.562 0.489	**IIIcf** [a)]	Cu—O_{16a} Cu—O_{17}	0.610 0.518
O_{17}, O_{21}	–	–	–	**IIef1**	Cu—O_{17} Cu—O_{21}	0.584 0.603	**IIIef**	Cu—O_{17} Cu—O_{21}	0.608 0.679
	–	–		**IIef2**	Cu—O_{17} Cu—$O(H)_{21}$ Cu—C_{18}	0.540 0.084 0.230	–	–	–

[a)]CO_2 release

Tab. 6. MPA charges and spin populations of Cu atoms in model complexes of Cu with lactone (**I**), carboxyl (**II**) and carboxylate (**III**) ligands (see Fig. 1 for atom notation).

	I (Steklac and Breza, 2022)			**II**			**III** $^-$		
Site	Model	Charge	Spin	Model	Charge	Spin	Model	Charge	Spin
N_1	**Ia**	0.863	0.000	**IIa**	0.857	0.000	**IIIa**[a)]	0.836	0.000
O_{16a}	**Ic**	0.816	0.000	–	–	–	–	–	–
O_{20}	**Id**	0.918	0.001	–	–	–	**IIId**[a)]	1.040	0.315
O_{21}	**Ie**	0.821	0.000	**IIe**	0.934	0.001	**IIIe**	0.715	0.000
O_{10}	**Ig**	0.881	0.000	**IIg**	0.879	0.000	–	–	–
$O_{1'}$	**Ih**	0.999	0.002	**IIh**	0.999	0.000	**IIIh**[a)]	0.977	0.002
$N_{2'}$	**Ii**	0.846	-0.001	**IIi**	0.843	-0.001	**IIIi**[a)]	0.553	0.337
$N_{8'}$	**Ij**	0.803	0.000	**IIj**	0.802	0.000	**IIIj**[a)]	0.573	0.273
O_{16a}, O_{17}	–	–	–	**IIcf**	0.864	0.028	**IIIcf** [a)]	0.816	0.007
O_{17}, O_{21}	–	–	–	**IIef1**	0.829	0.001	**IIIef**	0.900	0.179
	–	–	–	**IIef2**	0.836	0.000	–	–	–
Average	–	0.878	0.000		0.871	0.003		0.801	0.139

[a)]CO_2 release

anionic carboxylate ligand, which is in agreement with the QTAIM data. Average MPA Cu charges are lower than in analogous forms of camptothecin (Steklac and Breza, 2021).

Conclusions

Our results indicate high similarity between active and inactive forms of camptothecin (Steklac and Breza, 2021) and irinotecan. In both cases, no Cu—N_4 bonds were found and the Cu—O_{17} bond is absent in the complexes of the neutral lactone ligand. The formation of Cu(II) complexes with the anionic carboxylate ligand leads to the release of CO_2 in both cases. This corresponds to the interaction with electron acceptors in real solutions and the decrease in the concentration of lactone forms because of the equilibria between all forms of the drug. Absolute values of interaction energies and electron density transfer to Cu increase in the sequence lactone < neutral carboxyl < anionic carboxylate. In analogy with our studies on substituted phenols and quinones (Steklac and Breza, 2021a, 2021b, 2021c), cytotoxicity should exhibit the same trend. Both neutral forms of irinotecan exhibit more negative interaction energies than those of camptothecin, unlike the anionic carboxylate form. The lowest electron density transfer irinotecan → Cu is from $N_{2'}$, $N_{8'}$, and O_{10} sites which are not present in camptothecin.

We plan to extend the above studies to other camptothecin derivatives and their forms to contribute to better understanding the electronic structure factors of drug cytotoxicity that cannot be distinguished from pharmacokinetic factors in the experimental data.

Acknowledgments

This work was supported by the Slovak Grant Agency VEGA (contract No. 1/0139/20) and by the Slovak Science and Technology Assistance Agency (contract no. APVV-20-0213). The authors thank the HPC center at the Slovak University of Technology in Bratislava, which is a part of the Slovak Infrastructure of High Performance Computing (SIVVP Project No. 26230120002, funded by the European Region Development Funds), for computing facilities. M.B. thanks the Ministry of Education, Science, Research and Sport of the Slovak Republic for funding within the scheme 'Excellent research teams'.

References

Alagona G, Ghio C (2009) J Phys Chem A 113: 15206–15216.

Alagona G, Ghio C (2009a) Phys Chem Chem Phys 11: 776–790.

Babu PC, Sundaraganesan N, Sudha S, Aroulmoji V, Murano E (2012) Spectrochim Acta A 98: 1–6.

Bader RFW (1990) Atoms in Molecules: A Quantum Theory. Claredon Press, Oxford.

Bailly Ch (2019) Pharmacol Res 148: 104398.

Becke AD (1993) J Chem Phys 98: 5648–5652.

Biegler-Konig F, Schonbohm J, Bayles D (2001) J Comput Chem 22: 545–559.

Breza M (2021) Acta Chim Slovaca 14: 38–50.

Breza M, Jelemenska I (2022) J Vinyl Addit Technol 28: 352–366.

Breza M, Simon P (2019) Acta Chim Slovaca 12: 168–174.

Breza M, Simon P (2020) J Nanopart Res 22: 0058.

D'Amelio N, Aroulmoji V, Toraldo A, Sundaraganesan N, Anbarasan PM (2012) J Mol Struct 1013: 26–35.

DiNunzio MR, Douhal Y, Organero JAG, Douhal A (2018) Phys Chem Chem Phys 20: 14182–14191.

Fassberg J, Stella VJ (1992) J Pharm Sci 81: 676–684.

Frisch MJ, Trucks GW, Schlegel HB, Scuseria GE, Robb MA, Cheeseman JR et al. (2013) Gaussian 09, Revision D.01, Gaussian, Inc., Wallingford, CT.
Hussain I, Bania KK, Gour NK, Deka RC (2016) ChemistrySelect 1: 4973–4978.
Ivanova B, Spiteller M (2012) J Mol Struct 1012: 189–197.
Jelemenska I, Breza M (2021) Polym Degrad Stab 183: 109438.
Kabanda MM, Tran VT, Seema KM, Serobatse KRN, Tsiepe TJ, Tran QT, Ebenso EE (2014) Mol Phys 113: 683–697.
Keith TA (2017) AIMAll, Version 17.11.14, TK Gristmill Software Overland Park, KS. Available from aim.tkgristmill.com.
Mammino L (2013) J Mol Model 19: 2127–2142.
Mulliken RS (1955) J Phys Chem 23: 1833–1840.
Mulliken RS (1955a) J Phys Chem 23: 1841–1846.
Puskarova I, Breza M (2016) Polym Degrad Stab 128: 15–21.
Puskarova I, Breza M (2017) Chem Phys Let 680: 78–82.
Sawada S, Okajima S, Aiyama R, Nokata K-I, Furuta T, Yokokura T, Sugino E, Yamaguchi K, Miyasaka T (1991) Chem Pharm Bull 39: 1446–1454.
Serobatse KRN, Kabanda MM (2016) Eur Food Res Technol 242: 71–90.
Serobatse KRN, Kabanda MM (2016a) J Theor Comput Chem 15: 1650048.
Steklac M, Breza M (2018) Acta Chim Slovaca 11: 6–10.
Steklac M, Breza M (2021) Comput Theor Chem 1206: 113461.
Steklac M, Breza M (2021a) Polyhedron 207: 115360.
Steklac M, Breza M (2021b) ChemistrySelect 6: 7049–7055.
Steklac M, Breza M (2021c) Polyhedron 210: 115532.
Steklac M, Breza M (2022) Comput Theor Chem 1211: 113677.
Steklac M, Breza M (2022a) Acta Chim Slovaca 15: 72–84.
Tanizawa A, Fujimori A, Fujimori Y, Pommier Y (1994) J Natl Cancer Inst 86: 836–842.
Tsiepe TJ, Kabanda MM, Serobatse KRN (2015) Food Biophys 10: 342–359.
Ugliengo P (2006) MOLDRAW: A Program to Display and Manipulate Molecular and Crystal Structures. University Torino, Torino. Available from: www.moldraw.software.informer.com.